Correction of Excessive Precipitation over Steep and High Mountains in a GCM: A Simple Method of Parameterizing the Thermal Effects of Subgrid Topographic Variation

Winston C. Chao

Global Modeling and Assimilation Office

NASA/Goddard Space Flight Center

Greenbelt, Maryland 20771

(Revised January 30, 2015)

Corresponding Author Address:
Dr. Winston C. Chao
Mail Code 610.1
NASA/Goddard Space Flight Center
Greenbelt, MD 20771
Winston.c.chao@nasa.gov

Abstract

The excessive precipitation over steep and high mountains (EPSM) in GCMs and meso-scale models is due to a lack of parameterization of the thermal effects of subgrid-scale topographic variation. These thermal effects drive subgrid-scale heated-slope-induced vertical circulations (SHVC). SHVC provide a ventilation effect of removing heat from the boundary layer of resolvable-scale mountain slopes and depositing it higher up. The lack of SHVC parameterization is the cause of EPSM. The author has previously proposed a method of parameterizing SHVC, here termed SHVC.1. Although this has been successful in avoiding EPSM, the drawback is that it suppresses convective-type precipitation in the regions where it is applied.

In this article we propose a new method of parameterizing SHVC, here termed SHVC.2. In SHVC.2, the potential temperature and mixing ratio of the boundary layer are changed when used as input to the cumulus parameterization scheme over mountainous regions. This allows the cumulus parameterization to assume the additional function of SHVC parameterization. SHVC.2 has been tested in NASA/Goddard's GEOS-5 GCM. It achieves the primary goal of avoiding EPSM while also avoiding the suppression of convective-type precipitation in regions where it is applied.

1. Introduction

Excessive precipitation over steep and high mountains (EPSM), has until recently been a problem common to all GCMs (e.g., Fig. 1 of Ma et al. 2011) and meso-scale models (see, e.g., da Rocha et al. 2009). It occurs principally over the Andes in the DJF season and over the Himalayas and to their east in the JJA season, and--in models where this problem is more severe--over Mexico, Borneo, New Guinea, and the Ethiopian Highlands. Moreover, EPSM is also present in the current super parameterization (SP, or multi-modeling framework MMF) models (Tao et al. 2009) and has propagated into data assimilation products (da Rocha et al. 2009, and Fig. 3 of Bosilovich et al. 2011).

The cause of EPSM was identified as not recognizing the importance of the thermal effects of subgrid-scale topographic variation on deep convection (Chao 2012, hereafter C12),[1] and thus not parameterizing these effects in the models. In contrast, the importance of the corresponding mechanical effects has long been recognized and they are included in the GCMs as the envelope topography, blocked flow drag and as a part of the gravity wave parameterization.

Subgrid-scale topographic variation, which is large on the slopes of resolvable high mountains, creates subgrid-scale heated-slope-induced vertical circulations (SHVC) when the surfaces of the subgrid-scale mountain

[1] In current SP/MMF models the cloud models used have flat bottoms and thus are unable to simulate the thermal effects of the topographic variation.

slopes are heated during the day by solar radiation. SHVC takes heat out of the boundary layer on the resolvable-scale mountain slopes and deposits it higher up. Also, SHVC may trigger cumulus convection. Without the ventilation effect of SHVC parameterization, the model boundary layer on resolvable-scale steep slopes of high mountains is heated excessively during the day. The resulting excessive upslope boundary layer flow brings excessive amounts of moisture up from the lower levels of the mountain slopes, leading to excessive grid-scale (also called large-scale or resolvable-scale) precipitation, i.e., EPSM. The heat released in the excessive grid-scale precipitation enhances the heating in the boundary layer on the resolvable slopes and thus the upslope flow and creates a positive feedback.

Naturally, as the model horizontal resolution is increased, more of the previously-unresolved SHVC circulation is resolved, and therefore, the severity of EPSM diminishes. Like gravity wave parameterization, SHVC parameterization is not needed if the horizontal resolution is very high, likely as high as a 1-km grid size. Recent results from NASA's Goddard Earth Observing System GCM version 5 (GEOS-5 GCM) with a 7-km grid size still show recognizable EPSM (see also, Iga et al. 2007). Since the widespread use of global models with a 1-km horizontal grid size is still far in the future, the need for SHVC parameterization remains. Although there has been significant progress in the study of SHVC (e.g., Kirshbaum 2013 and the references therein), the development of SHVC parameterization is still in its early stage.

C12 proposed a crude method of parameterizing SHVC by taking most of the heat received in the boundary layer from surface sensible-heat flux and redistributing it to layers high above the boundary layer, well into the upper troposphere, in regions where subgrid-scale topographic variation is large. These regions coincide with regions of steep and high mountains. With respect to moisture, it is assumed that the fraction of moisture per time step taken out of the boundary layer by SHVC is proportional to the fraction of heat taken out of the boundary layer. The proportionality constant α is determined by tuning. We will see shortly that this treatment of moisture should be changed. Nothing is done for momentum. C12 has argued that not doing anything for momentum is acceptable as far as avoiding EPSM is concerned.

C12's scheme of parameterizing SHVC, referred to hereafter as SHVC.1, succeeded in avoiding the EPSM problem. However, by removing heat and moisture from the boundary layer and redistributing them to higher levels, SHVC.1 stabilizes the atmospheric column and thus suppresses cumulus convection in the regions where it is applied. As a result, the reduction in precipitation by SHVC.1 over mountainous regions comes mostly from the convective type of precipitation and most of the grid-scale (also called large-scale) precipitation--which forms mostly in the bottom layers of the model--remains. Consequently, grid-scale precipitation--rather than convective precipitation--predominates over high mountains, even for model horizontal grid sizes as large as 2 degrees. This is contrary to

observations (Bhatt and Nakamura 2005, Fig. 8 of Shrestha et al. 2012). In addition, since the cumulus transport of momentum depends on convective fluxes, it is also negatively impacted by SHVC.1.

In this article we propose a new method of parameterizing SHVC, termed SHVC.2. Besides achieving the primary objective of avoiding EPSM, SHVC.2 also avoids the problem of suppressing convective-type precipitation in regions where it is applied. Section 2 describes the details of SHVC.2. Some test results using NASA/Goddard's Goddard Earth Observing System GCM version 5 (GEOS-5 GCM) are shown in Section 3. Section 4 is a discussion and summary.

2. SHVC.2

The main function of SHVC parameterization is to remove heat from the boundary layer and deposit it higher up, in regions with high subgrid-scale topographic standard deviation μ, which coincide with regions of steep slopes of resolvable high mountains. This function can also be performed by cumulus parameterization after a simple modification. Thus, a new method of SHVC parameterization, termed SHVC.2, allows cumulus parameterization to be more active than when SHVC.1 is used in a way such that a sufficient amount of heat is removed from the boundary layer by cumulus parameterization in regions where μ is large. The idea of SHVC.2 is that, in the regions where μ is large, the potential temperature θ and water vapor

mixing ratio q at the cumulus initiation level (the level representing the PBL) are changed when the cumulus parameterization scheme is used. These changes occur only when θ and q are used as input into the cumulus parameterization scheme.[2] These changes do not directly affect these quantities themselves. They take the forms of:

$$\Delta\theta_K = F_\theta F_\mu \qquad (1)$$

$$\Delta q_K = F_q F_\mu \qquad (2)$$

where θ_K and q_K are the potential temperature (°K) and the water mixing-ratio (kg/kg) of a super layer representing the boundary layer, respectively.

In GEOS-5 several levels may reside within the boundary layer. After the determination of the layer K whose top is identified as the top of the PBL, and before the cumulus parameterization is called, a super layer, which is a strapping of level K and all levels below it, is formed. The properties of the super layer are mass-weighted averages of the properties of level K and the levels below it. The super layer represents the mixed boundary layer for the purpose of computation of the cumulus parameterization and is given the

[2] Before calling the cumulus parameterization scheme the profiles of θ and q are saved. Next, the θ and q at the cloud initiation level are modified according to these changes and then used as input for the cumulus parameterization scheme. The changes in θ and q computed by the cumulus parameterization scheme are then added to the saved θ and q profiles to obtain the updated profiles.

level index of K. Level K is the cloud-originating level. The rate of static energy taken out of the boundary layer by the cumulus parameterization scheme is equal to the dry static energy S computed from θ_K and the height of level K times the cumulus mass flux rate at level K-$_{1/2}$, M_c, subtracting the static energy at level K-$_{1/2}$ multiplied by the compensating downward mass flux, also M_c, at level K-$_{1/2}$, the edge level between layers K and K-1; i.e., $-M_c(S_K - S_{K-1/2})$. See Fig. A1 in Appendix A, which is similar to Fig. A1 of Moorthi and Suarez (1992), for an illustration of the levels.

F_θ = 12°K and F_μ = 0 when μ < 300 m and F_μ = 1 when μ > 400 m. In between a linear interpolation is performed. Both factors were determined by experimentation. Thus, SHVC.2 is applied only when μ is greater than 300m. We set F_q = -0.1 q_k through experimentation. The negative value means moisture is transported into the boundary layer from above by SHVC. We will explain this shortly.

We also tried multiplying an F_Z factor (F_Z = max (cosZ, 0.)) to the right-hand sides of Eqs. (1) and (2). F_Z accounts for the solar angle factor, where Z is the solar zenith angle with a 2-hour delay. The 2-hour delay reflects the time it takes SHVC to respond to surface heating. However, using F_Z would require F_θ to be set at a much larger value in order to suppress EPSM. Thus, in the experiments reported below, the F_Z factor was not used.

$\Delta\theta_K$ is only a device to make cumulus parameterization more active than when SHVC.1 is used and to ensure that a sufficient amount of heat is

176 removed from the boundary layer by the cumulus parameterization in
177 regions where μ is large. The argument for increasing θ_K is as follows.
178 Within a grid, related to the SHVC, there are subgrid-scale topographic
179 variations and heat advection in the boundary layer on subgrid slopes. As a
180 consequence, the boundary layer temperature is not horizontally-uniform (in
181 terrain-following coordinates) and thus there are spots within the grid,
182 corresponding to the peaks of subgrid topography, that have local peak
183 potential temperatures that are greater than the grid mean. It is from these
184 spots that cumulus convection originates. Therefore, it is justifiable to give
185 the potential temperature at the cloud initiation level a boost when using
186 cumulus parameterization in regions where μ is large.

187 In our design, θ and q at the levels above level K are not changed. This
188 may seem inconsistent with the justification of changing θ and q at level K.
189 However, not changing θ and q at levels above K is necessary to ensure that
190 heat is efficiently removed from the boundary layer by the cumulus
191 parameterization scheme. The obvious advantage of SHVC.2 over SHVC.1 is
192 that the problem of convective precipitation being suppressed is mostly, if
193 not totally, avoided.

194 Letting cumulus parameterization pick up the additional function of
195 SHVC parameterization has conceptual appeal because SHVC itself is not
196 necessarily a dry convection. The upward branch of the SHVC circulation can
197 turn into cumulus convective circulation, and the two types of circulation are

198 in fact closely intertwined over mountainous regions. It thus makes more
199 sense to combine them than to treat them separately.

200 While SHVC transports heat out of the boundary layer over grids with
201 large μ, it does the opposite for moisture (as seen from the results of a 7-km
202 grid GCM simulation; M. Suarez, personal communication), contrary to what
203 was proposed in C12. This can be explained as follows. Fig. 1 shows that
204 because moisture decreases exponentially with height--unlike potential
205 temperature, which increases with height--in the SHVC circulation, the air
206 mass entering the boundary layer at low levels is moister than that exiting
207 the boundary layer at high levels. Surface sensible-heat flux helps increase
208 the potential temperature of the air exiting the boundary layer at peaks of
209 the subgrid topography, but evaporation on the subgrid-scale mountain
210 slopes is not strong enough to make the air exiting the boundary layer at high
211 levels moister than the air entering the boundary layer at low levels. This
212 explains our negative change to q_K.

213 Should changes to momentum in the PBL similar to the changes in θ_K
214 and q_K also be made? The changes to θ_K and q_K are made for the purpose of
215 letting cumulus parameterization take on the additional function of SHVC
216 parameterization, but momentum is not a factor in this purpose. Thus, for
217 simplicity such a change to momentum was not made. The transport of
218 momentum by the cumulus parameterization is done following the existing
219 method in RAS (the relaxed Arakawa-Schubert scheme (Moorthi and Suarez
220 1992)): momentum is transported by cumulus mass fluxes (and entrainment

and detrainment) computed by RAS. Thus, in both SHVC.1 and SHVC.2 the change in convective precipitation—and thus in cumulus fluxes--impacts momentum transport. As explained in C12, since adding or subtracting friction on the slopes of high mountains has little impact on EPSM, the transport of momentum by SHVC is not a major factor in avoiding EPSM. Therefore, the impact on momentum transport, whether due to the use of either SHVC.1 or SHVC.2, has little effect on EPSM.

One may wonder that if SHVC.1 and SHVC.2 yield similar heating and moistening rate profiles due to SHVC whether the partitioning of precipitation between convective type and large-scale type really makes any difference. The answer is that different impacts on cloudiness by the two approaches makes a difference in the radiative heating rates. In addition, since the cumulus transport of momentum is through cumulus fluxes, SHVC.1, with its suppression of convective precipitation, suppresses such transport, whereas SHVC.2 does not. This is another advantage of SHVC.2.

3. The model and test results

As in C12, we used the GEOS-5 GCM with a 2° (lat) by 2.5° (lon) horizontal grid size and 72 vertical levels. The EPSM problem is most severe at this horizontal grid spacing, thus making this resolution the best for testing SHVC schemes. With a larger grid size, the slopes of the resolvable mountains are smaller and thus the EPSM problem is less severe. With

244 smaller grid sizes, more short-scale mountains are resolved, which can allow
245 some of the ventilation effect to be simulated, thereby lessening the EPSM
246 problem. A brief description of the model was given in C12 and Chao (2013,
247 hereafter C13) and is thus not repeated here. (A detailed description of the
248 GEOS-5 model used in C12's work is given in Molod et al. (2012).)

249 There have been three new revisions to the model since C12. The first
250 was Molod's (2012, hereafter M12) modification to lower the critical relative
251 humidity for large-scale precipitation to occur. The M12 modification results
252 in a better simulation of the relative humidity field but it enhances peak
253 large-scale precipitation and enlarges the areas that have low large-scale
254 precipitation in the climatological state of the model. Because it enhances
255 peak large-scale precipitation over high mountains, the M12 modification
256 makes the EPSM problem somewhat more severe.

257 As a second revision, the catastrophe-concept-based cumulus
258 parameterization (C-CUP) of C13 is used over land to improve the simulation
259 of the precipitation diurnal cycle. The relaxed Arakawa-Schubert cumulus
260 parameterization (RAS) (Moorthi and Suarez 1992) is retained over the
261 ocean in this work. C13 has shown that C-CUP applied over both land and
262 ocean yields a larger bias in the mean state than when it is applied over land
263 only. This could be because the parameter settings in C-CUP were tuned for
264 land and are not suitable over the ocean. The tuning work for C-CUP over the
265 ocean has yet to be completed. C-CUP does not have any significant impact
266 on EPSM.

The third revision is a new microphysics package (Barahona et al. 2014), which includes modifications to both large-scale and convective moist processes. This new microphysics package enhances convective precipitation and reduces large-scale precipitation. It reduces peak large-scale precipitation (in regions including high mountains) and more than compensates for the increase due to M12, thus making the EPSM problem much less severe in GEOS-5. GEOS-5 previously had an EPSM problem much more severe than most other GCMs. The new microphysics package reduces the severity of EPSM in the GEOS-5 GCM to a level more in line with other GCMs, although it is still among the highest of all the GCMs. All three revisions are used in this work.

We should also note that before these revisions were included, the model already had a $\Delta\theta_K$ of 2°K applied to all grid columns. This increase was empirically determined to improve model performance. It can be somewhat justified by the subgrid inhomogeneity and the imperfection of the cumulus parameterization scheme, and was retained in our experiments.

We conducted three experiments with 1) no SHVC, 2) SHVC.1 and 3) SHVC.2, each of 5-year duration beginning on May 29th of 2002. In SHVC.1 heat was removed from the boundary layer over grids with high subgrid-scale topographic variation and redistributed higher up as described in C12. The α factor, defined on page 1552 of C12, is set at 1. (According to our earlier discussion it should be set at a negative value. We will discuss this at the end of this section.) The other methods of treating EPSM suggested in

290 C12 were not used. Due to the reduction in the severity of EPSM in GEOS-5
291 through the use of the new microphysics package, there was no need to
292 remove as large an amount of heat from the boundary layer as described in
293 C12 when SHVC.1 was used. We have, therefore, reduced the R_S factor, as
294 specified in Fig. 5 of C12, by 20% in SHVC.1.

295 Fig. 2 shows the 5-year-averaged precipitation difference from the
296 GPCP data for the three experiments in the Dec-Jan-Feb (DJF) and Jun-Jul-
297 Aug (JJA) seasons. In noSHVC the EPSM problem was less severe than what
298 was reported in C12. For example, Fig. 2 shows that the EPSM problem over
299 the Himalayas and the regions to its east in JJA was less severe than what was
300 shown in E001 in the bottom panel of Fig. 8b of C12. Over the Andes in DJF
301 there was a similar outcome in noSHVC (Fig. 2, upper panel). Also, in JJA the
302 EPSM problem disappeared over New Guinea, Mexico and the Ethiopean
303 Highlands (cf., Fig. 8 of C12). As we mentioned earlier, these results can be
304 attributed to the use of the new microphysics package, since a similar
305 experiment (not shown) without the new microphysics package had an EPSM
306 problem just as severe as what was reported in C12. Fig. 2 also shows that
307 SHVC.2 has achieved the goal of avoiding EPSM, although there was a small
308 remnant over the Andes in DJF. Both SHVC.1 and SHVC.2 had no significant
309 impact on the ITCZ bias.

310 Figs. 3 and 4 show the 5-year-averaged sum of the convective and
311 anvil types of precipitation (upper panel); the large-scale type of
312 precipitation (middle panel); and their difference (bottom panel), which

313 equals the middle panel minus the upper panel for the three experiments in
314 DJF and JJA, respectively. These figures show that the sum of convective and
315 anvil types of precipitation over the Himalayas and regions to its east in JJA
316 and over the Andes in DJF was significantly smaller than the large-scale type
317 of precipitation in SHVC.1 but not in SHVC.2. Thus, the problem of
318 suppression of convective precipitation over the EPSM areas caused by
319 SHVC.1 has been avoided by using SHVC.2. Student's t significance tests
320 show that the results shown in Fig. 2 through 4 are statistically meaningful
321 over the mountainous regions where SHVC.1 or SHVC.2 is applied. See the
322 Appendix B for details.

323 Results of the difference in sea level pressure, 500 hPa height and 300
324 hPa temperature from their respective MERRA analysis fields (Rienecker et
325 al. 2011) are shown in Figs. 5 through 7. Both SHVC.1 and SHVC.2 have a
326 comparable or better performance than noSHVC.

327 Table 1 shows the standard deviation of the error in various fields,
328 with the error defined as the difference from the MERRA analyses (with the
329 GPCP data for precipitation), averaged over JJA and DJF and over the five
330 years for the three experiments. The small improvement of SHVC.1 over
331 noSHVC is generally sustained in SHVC.2. In the fields where SHVC.2
332 performs worse than noSHVC, the degradation is not significant.

333 In an additional experiment with SHVC.1 we set $\alpha = -0.1$. This
334 experiment showed successful suppression of EPSM similar to the $\alpha = 1$ case
335 but the dipole error pattern in the JJA 500-hPa-height error field in the

middle and high latitudes over the Southern Hemisphere as shown in noSHVC (lower left panel of Fig. 6) becomes more than noticeably worse than noSHVC (figure not shown). We have no explanation for this adverse outcome.

4. Discussion and summary

Even with the use of the new microphysics package, the EPSM problem in the GEOS-5 GCM (without using SHVC parameterization) is still among the GCMs that have the worst EPSM problem (compare Fig. 1 of Ma et al. (2011) with Fig. 2). This implies that the magnitudes of θ_K and q_K needed for SHVC.2 to overcome EPSM in the GEOS-5 GCM can be further reduced when other components of the model are further improved. However, as we discussed in the introduction, the need for SHVC parameterization will not disappear no matter how good the model is, unless the horizontal grid size is reduced to 1 km or less.

When used in other models or used with a different grid size, SHVC.2 requires re-tuning of its parameters, but its simple design makes such a task less onerous.

Both SHVC.1 and SHVC.2 can be used in SP/MMF models. SHVC.1 can be used in their host models and SHVC.2 can be used in the cloud-resolving models by changing the potential temperature and moisture in the boundary layer. But, a better way to solve the EPSM problem in SP/MMF models is to

359 allow topographic variation in the cloud-resolving models that are used and
360 to explicitly resolve SHVC.

361 The precipitation diurnal cycle over high mountains has been a
362 challenging problem for GCM simulations, as discussed in C13. This problem
363 has not been solved by the use of SHVC.2. We will leave this problem to a
364 future study.

365 In summary, this study has demonstrated that through some simple
366 modifications, cumulus parameterization can assume the function of SHVC
367 parameterization. Besides achieving the goal of removing the EPSM problem,
368 this new method of SHVC parameterization has the added advantage of
369 avoiding suppression of convective-type precipitation. This latter advantage
370 also avoids the negative impact on the cumulus transport of momentum over
371 the regions where SHVC parameterization is applied.

372 Undoubtedly SHVC parameterization research will continue. The
373 basic contribution of this work is that it offers a new direction—combining
374 SHVC parameterization with cumulus parameterization.

375

376 *Acknowledgments*. Help from Larry Takacs, Matt Thompson, Joe Stassi,
377 Danifan Barahona, and Purnendu Chakraborty of NASA/GSFC/GMAO in using
378 the GEOS-5 GCM and programming advices is gratefully acknowledged.
379 Discussion with Max Suarez was useful. Jim Gass provided graphics support.
380 This work was supported by NASA under WBS 432938.11.01.04.01.06.
381 Computing resources supporting this work were provided by the NASA High-

382 End Computing (HEC) Program through the NASA Center for Climate Studies
383 (NCCS) at Goddard Space Flight Center. Maharaj Bhat of NASA/NCCS helped
384 with setting up the Fortran code for Student's t test.
385

Appendix A

Schematic diagram showing the lower levels of the model (Fig. A1)

Appendix B

Significance tests on the difference fields

Student's t tests were preformed on the daily total precipitation fields of the three experiments. The computer code used for the test is tutest.f from *Numerical Recipes* (Press et al. 2002.) Fig. A.2a shows the high probability, mostly over 99%, that the difference between the means of the total precipitation (averaged over the DJF seasons for the 5-year period) in noSHVC and SHVC.1 over the Andes, where SHVC.1 is applied, is statistically significant. In other words, the chance that the difference between the means over these regions can be attributed to the sample size being small is very low. Fig. A.2c shows the same plot for the JJA season. It shows very good significance over the eastern Himalayas and the regions to its east. Figs. A.2b and A.2d show the same plots for the noSHVC and SHVC.2 pair. The degrees of freedom are 458 for JJA and 448 for DJF. Similar tests for large-scale precipitation, the sum of convective and anvil precipitation and sea level pressure also show similarly good results.

References

Barahona, D., A. Molod, J. Bacmeister, A. Nenes, A. Gettelman, H. Morrison, V. Phillips, and A. Eichmann, 2014: Development of two-moment cloud microphysics for liquid and ice within the NASA Goddard Earth Observing System model (GEOS-5). *Geosci. Model Dev.* 7, 1733-1766. doi:10.5194/gmd-7-1733-2014.

Bhatt, B. C. and K. Nakamura, 2005: Characteristics of monsoon rainfall around the Himalayas revealed by TRMM precipitation radar. *Mon. Wea. Rev.*, **133**, 149-165.

Bosilovich, M. G., F. R. Robertson, and J. Chen, 2011: Global energy and water budgets in MERRA. *J. Climate*, **24**, 5721–5739,

Chao, W. C., 2012: Correction of Excessive Precipitation over Steep and High Mountains in a GCM. *J. Atmos. Sci.,* **69,** 1547-1561 doi:10.1175/JAS-D-11-0216.1.

Chao, W. C., 2013: Catastrophe concept-based cumulus parameterization: Correction of systematic errors in the precipitation diurnal cycle over land in a GCM. *J. Atmos. Sci.*. **70**, 3599-3614. doi: 10.1175/JAS-D-13-022.1.

---

da Rocha, R. P., C. A. Morales, S. V. Cuadra, and T. Ambrizzi, 2009: Precipitation diurnal cycle and summer climatology assessment over South America: An evaluation of Regional Climate Model version 3 simulations. *J. Geophys. Res.*, **114**, D10108, doi:10.1029/2008JD010212.

Iga, S., H. Tomita, Y. Tsushima, M. Satoh, 2007: Climatology of a nonhydrostatic global model with explicit cloud processes. *Geophys. Res. Lett.*, 34, L22814, doi:10.1029/2007GL031048.

Kirshbaum, D. J., 2013: On thermally forced circulations over heated terrain. *J. Atmos. Sci.,* **70**, 1690-1709.

Ma, H.-Y., C. R. Mechoso, Y. Xue, H. Xiao, C.-M. Wu, J.-L. Li, and F. De Sales, 2011: Impact of land surface processes on the South American warm season climate. *Climate Dyn*., **37**, 187– 203, doi:10.1007/s00382-010-0813-3.

Molod, A., 2012: Constraints on the profiles of total water PDF in AGCMs from AIRS and a high-resolution model. *J. Climate*, **25**, 8341-8352. doi: 10.1175/JCLI-D-11-00412.1

Molod, A., L. Takacs, M. Suarez, J. Bacmeister, I.-S. Song, and A. Eichmann, 2012. The GEOS-5 Atmospheric General Circulation Model: Mean climate and development from MERRA to Fortuna. *NASA Technical Report Series on Global Modeling and Data Assimilation, NASA TM—2012-104606*, Vol. **28**, 117 pp. Available at: http://gmao.gsfc.nasa.gov/pubs/tm/docs/Molod484.pdf

Moorthi, S., and M. J. Suarez, 1990: Relaxed Arakawa-Schubert: A parameterization of moist convection for general circulation models. *Mon. Wea. Rev.,* **120**, 978-1002.

Press, W. H., S. A. Teukolsky, W. T. Vetterling, and B. P. Flanery, 1992: *Numerical Recipes*, 2nd Ed. Cambridge U. Press.

Rienecker, M. M. and coauthors, 2011: MERRA: NASA's modern era retrospective analysis for research and applications. *J. Clim*. **24**, 3624-3648.

Shrestha, D., P. Singh, and K. Nakamura, 2011: Spatiotemporal variation of rainfall over the central Himalayan region revealed by TRMM precipitation radar. *JGR*, **117**, D22106. Doi:10.1029/2012JD018140.

Table 1 Standard deviation of error fields (error being the difference between model results and MERRA analysis (GPCP data for precipitation), eddy being the deviation from zonal mean) averaged over 5 years

Exp.	(no SHVC)	(SHVC.1)	(SHVC.2)
DJF			
Precip (mm/day)	1.564	1.673	1.670
500 hPa H (m)	25.87	22.90	23.17
500 hPa eddy H (m)	15.54	15.54	14.97
500 hPa T (°K)	1.148	1.213	1.182
SLP (hPa)	3.569	3.173	3.330
JJA			
Precip (mm/day)	2.074	2.006	2.038
500 hPa H (m)	23.72	21.24	20.03
500 hPa eddy H (m)	19.25	17.11	15.25
500 hPa T (°K)	1.531	1.499	1.482
SLP (hPa)	3.160	2.783	3.069

Figure Captions

Fig. 1. A schematic diagram depicting the different heights of the in-coming and out-going flow in the boundary layer associated with the SHVC.

Fig. 2. Differences of model seasonally averaged precipitation (mm/day) from GPCP data averaged over the 5-year integration period for the three experiments: noSHVC, SHVC.1 and SHVC.2, for the DJF season (upper panels) and for the JJA season (lower panels).

Fig. 3. Convective plus anvil precipitation (mm/day) (upper panel), large-scale precipitation (middle panel) and their difference (upper panel minus middle panel) averaged over the 5-year integration period for the three experiments for the DJF season. The vertical color bar is for the upper and middle panels. The horizontal color bar is for the lower panels.

Fig. 4. Same as Fig. 3 but for the JJA season.

Fig. 5. Differences of model sea level pressure (hPa) from that of MERRA analysis averaged over the 5-year integration period for the three experiments for the DJF season (upper panels) and for the JJA season (lower panels.)

520

521 Fig. 6. Same as Fig. 5 but for 500 hPa height (m).

522

523 Fig. 7. Same as Fig. 5 but for 300 hPa temperature (°K).

524 .

525 Fig. A1. Schematic diagram showing the lower levels of the model. The
526 prognostic quantities are carried at the dashed levels and their values
527 at the solid levels are interpolated from the dashed levels. Mc denotes
528 the cloud bass mass flux and the compensating mass flux in the cloud
529 environment. K-1/2 denotes the top of the PBL.

530 Fig. A2. Statistical significance test results. Shown are the probability that
531 the difference between the five-year means of the total precipitation
532 of SHVC.1 and noSHVC (left two plots) cannot be attributed to the
533 sample size being small for DJF and JJA. The same plots for the
534 difference between SHVC.2 and noSHVC are shown in the right two
535 plots.

536

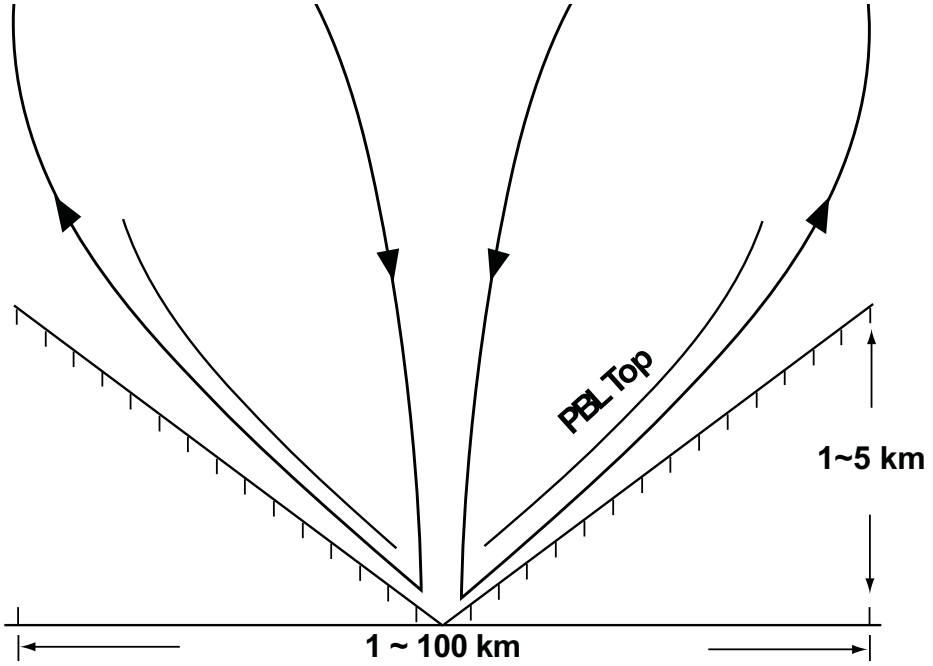

537

538 Fig. 1. A schematic diagram depicting the different heights of the in-coming

539 and out-going flow in the boundary layer associated with the SHVC.

540

541

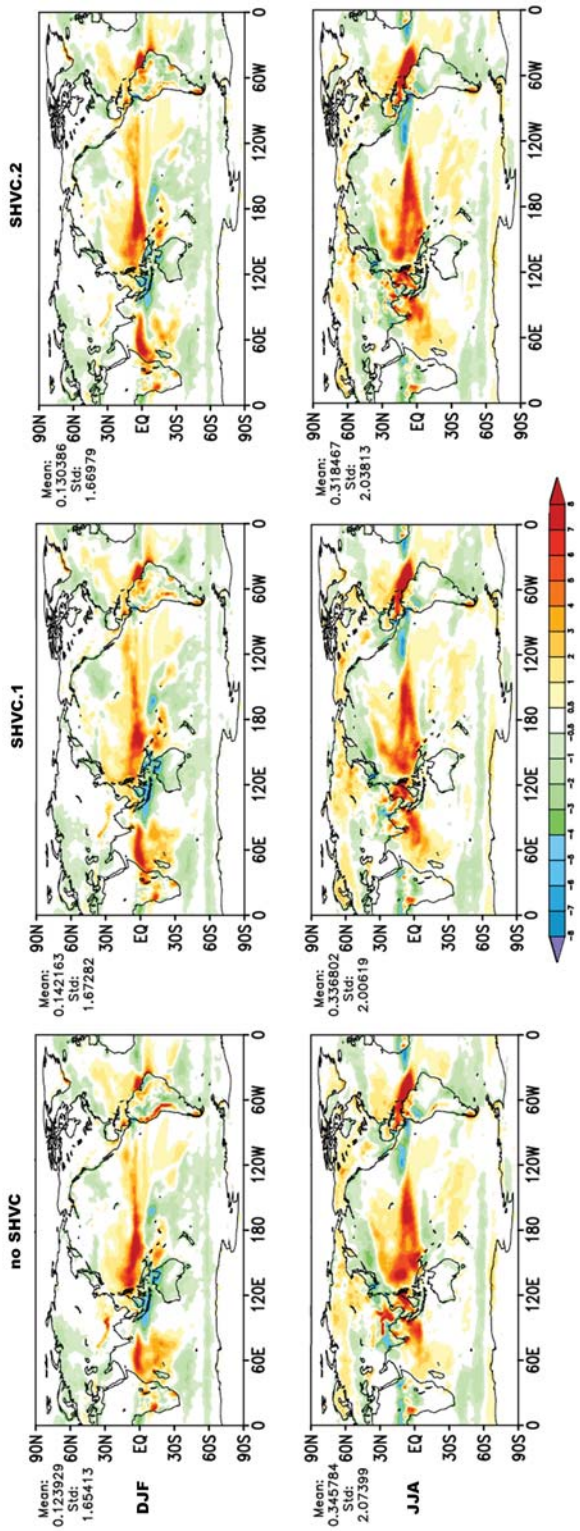

542

543 Fig. 2. Difference of model seasonally averaged precipitation (mm/day) from

544 GPCP data averaged over the 5-year integration period for the three

545 experiments: noSHVC, SHVC.1 and SHVC.2, for the DJF season (upper panels)
546 and for the JJA season (lower panels).
547

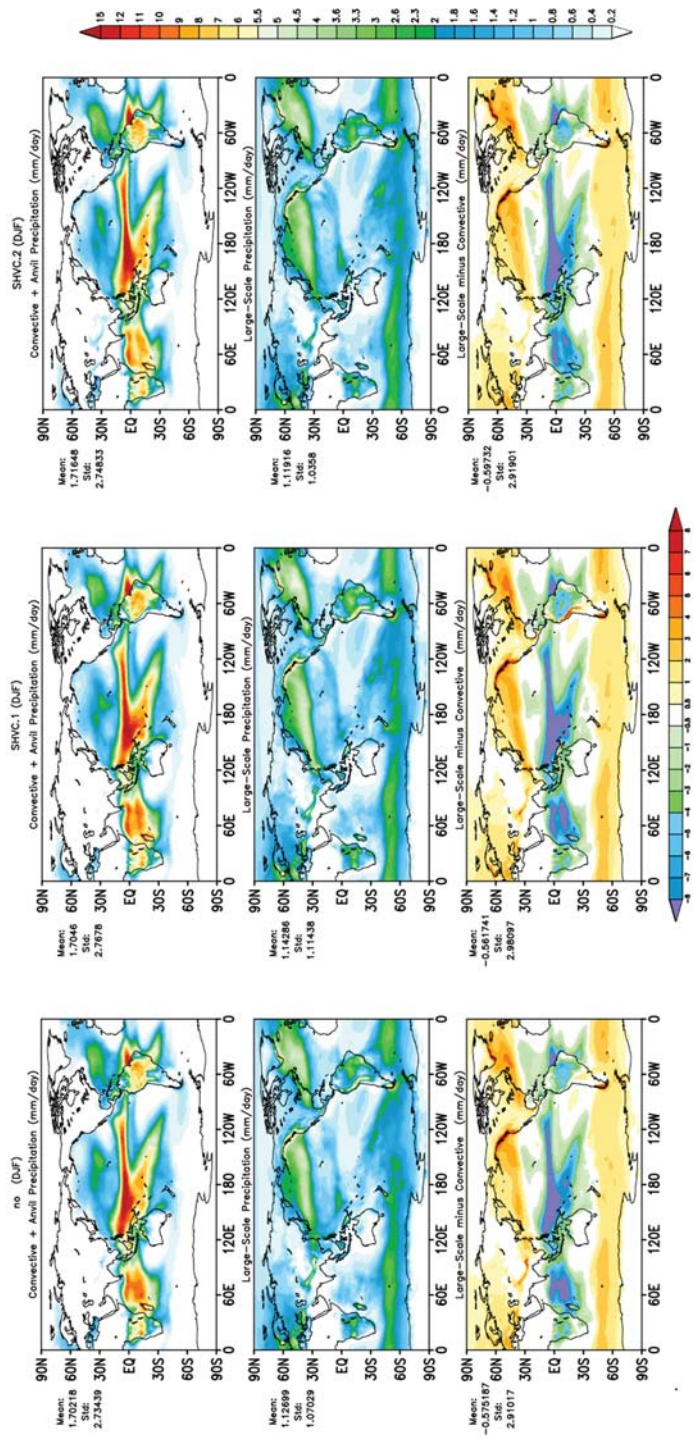

548

549 Fig. 3. Convective plus anvil precipitation (mm/day) (upper panel), large-

550 scale precipitation (middle panel) and their difference (upper panel minus

middle panel) averaged over the 5-year integration period for the three experiments for the DJF season. The vertical color bar is for the upper and middle panels. The horizontal color bar is for the lower panels.

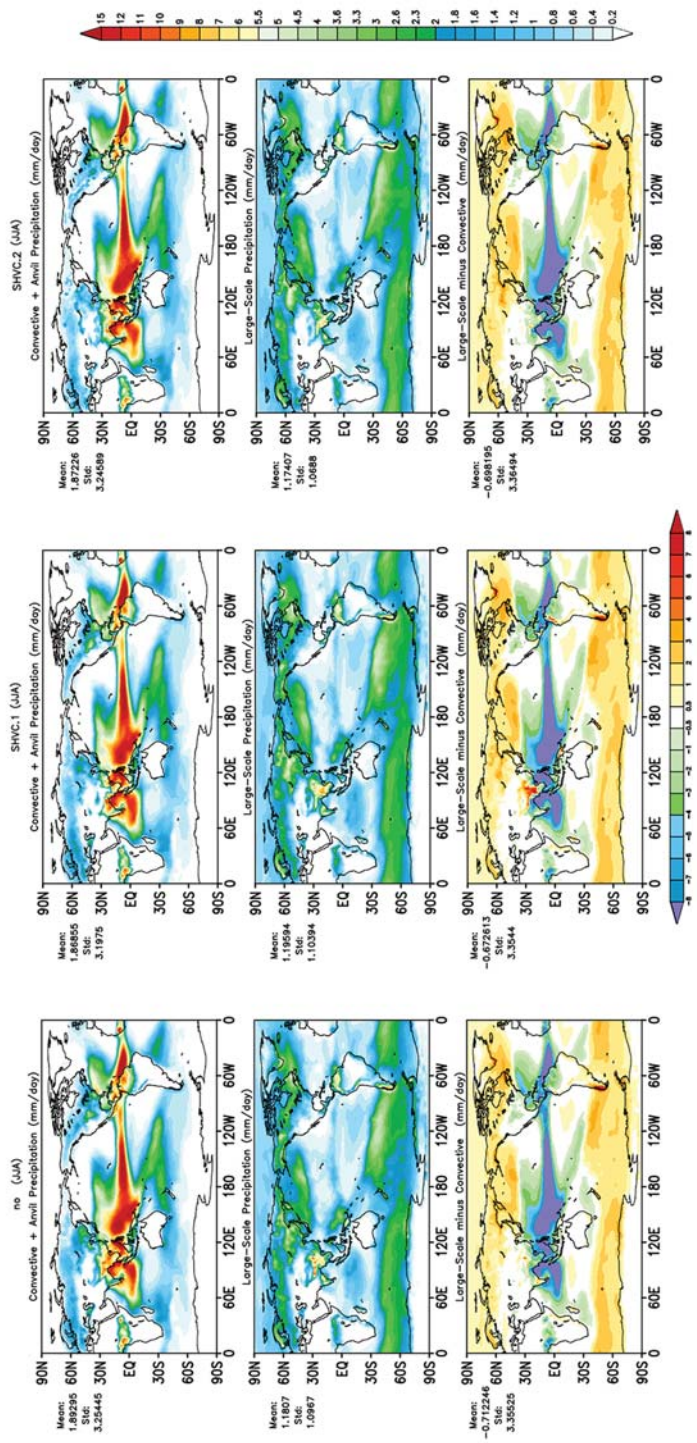

554

555 Fig. 4. Same as Fig. 3 but for the JJA season.

556

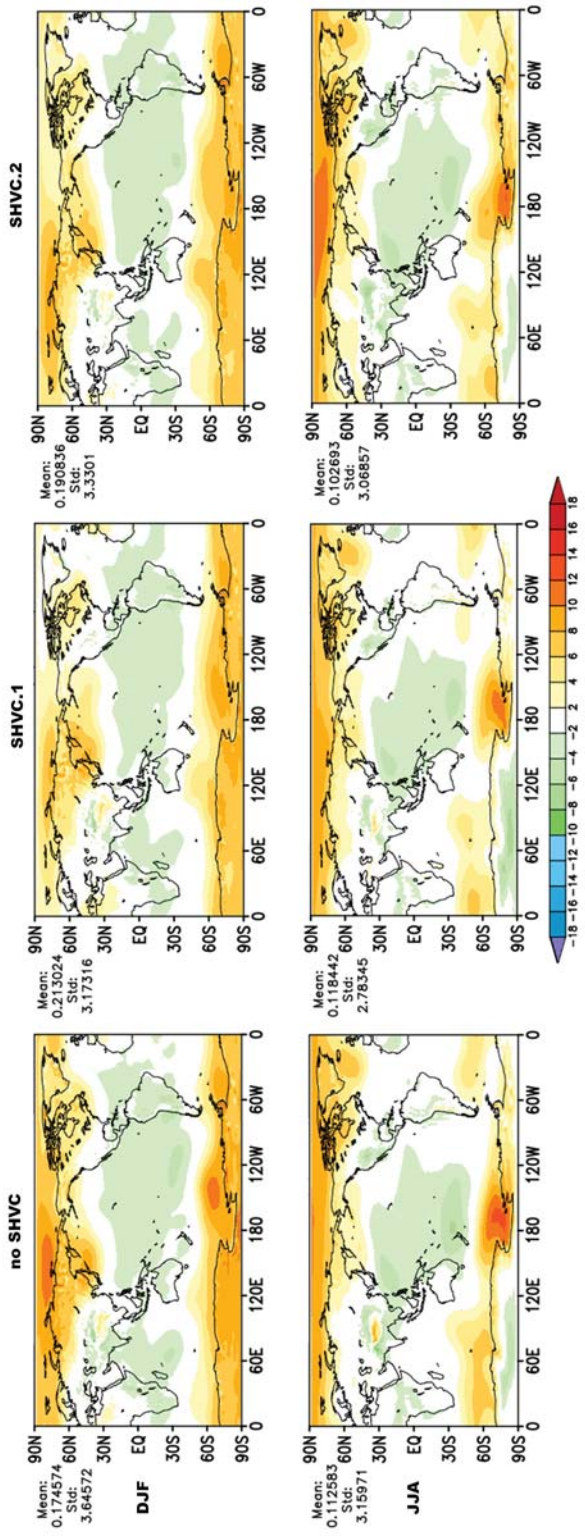

Fig. 5. Differences of model sea level pressure (hPa) from that of MERRA analysis averaged over the 5-year integration period for the three

560 experiments for the DJF season (upper panels) and for the JJA season

561 (lower panels.)

562

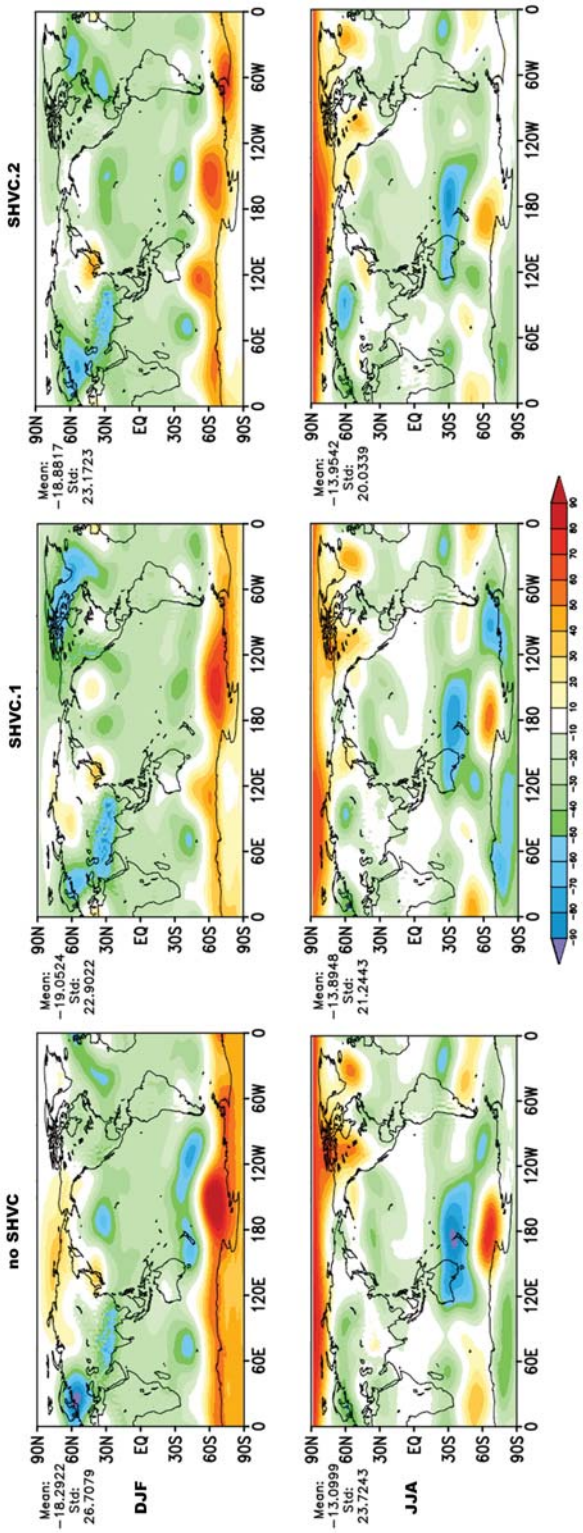

563 Fig. 6. Same as Fig. 5

564 but for 500 hPa height (m).

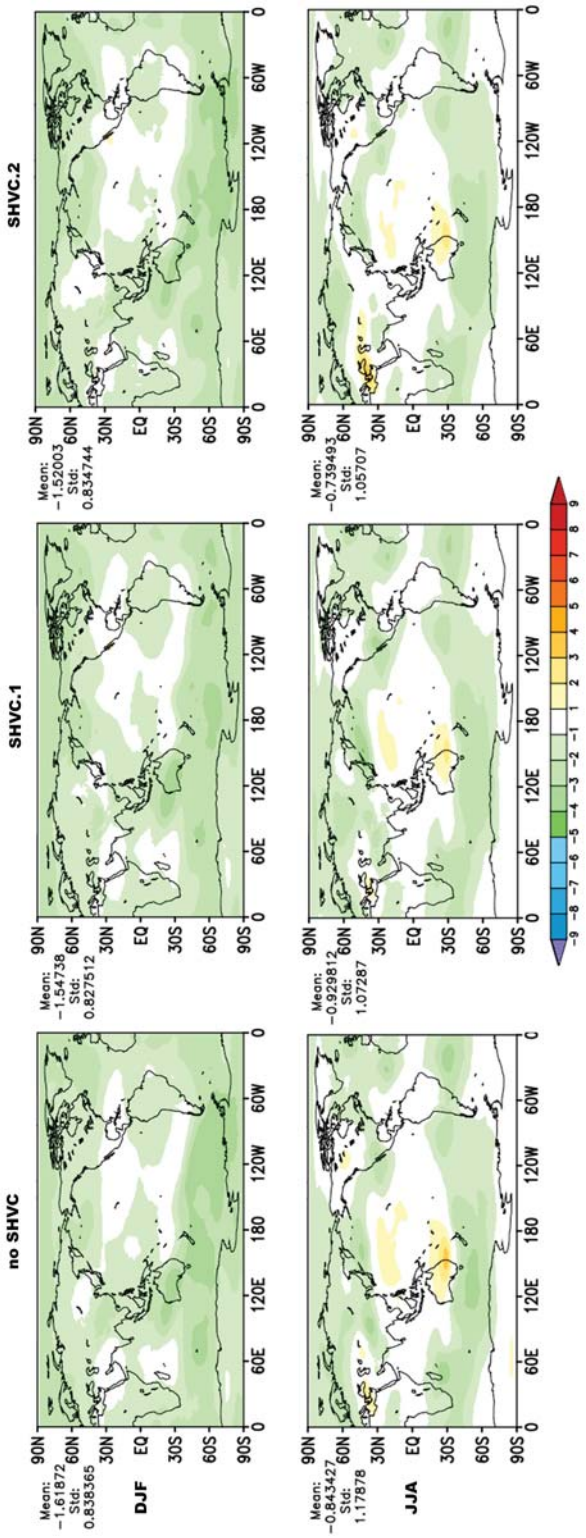

565

566 Fig. 7. Same as Fig. 5 but for 300 hPa temperature (°K).

567

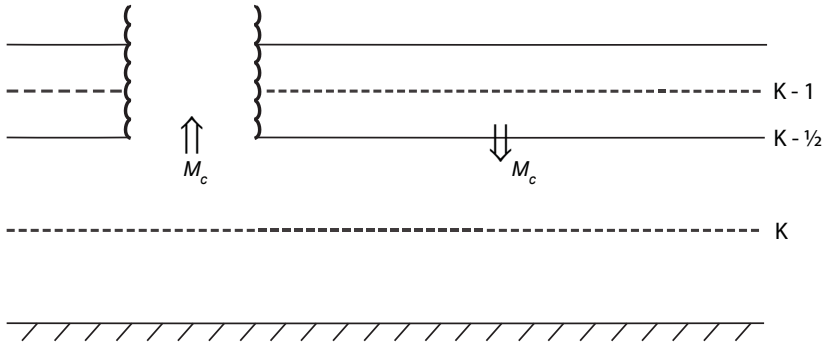

568

569

570 Fig. A1. Schematic diagram showing the lower levels of the model. The
571 prognostic quantities are carried at the dashed levels and their values
572 at the solid levels are interpolated from the dashed levels. *Mc* denotes
573 the cloud bass mass flux and the compensating mass flux in the cloud
574 environment. K-1/2 denotes the top of the PBL.

575

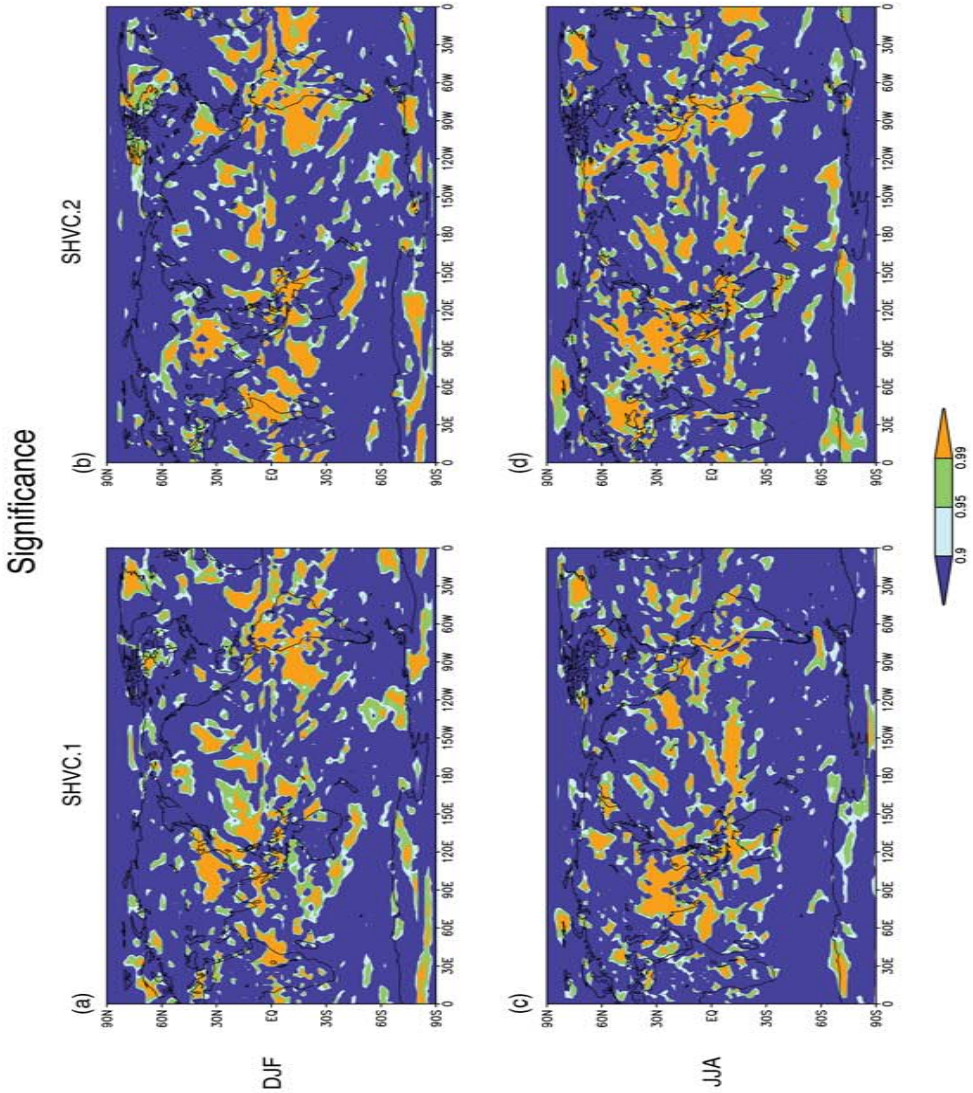

Fig. A2. Statistical significance test results. Shown are the probability that the difference between the five-year means of the total precipitation of SHVC.1 and noSHVC (left two plots) cannot be attributed to the sample size being small for DJF and JJA. The same plots for the

582 difference between SHVC.2 and noSHVC are shown in the right two
583 plots.
584